IOP Conf. Series: Materials Science and Engineering **219** (2017) 012036 doi:10.1088/1757-899X/219/1/012036

Tailoring hierarchical structures in selective laser melted materials

Jon Olsen[1], Xin Zhou[2], Yuan Zhong[1,2], Leifeng Liu[1], Dianzheng Wang[2], Chenfan Yu[2], Yafei Wang[2], Kailun Li[2], Leilei Xing[2], Jing Ma[2], Daqing Cui[1], Wei Liu[2]*, Zhijian Shen[1,2]*

[1] Department of Materials and Environmental Chemistry, Arrhenius Laboratory, Stockholm University, S-106 91 Stockholm
[2] School of Materials Science and Engineering, Tsinghua University, Beijing 100084, China

* Corresponding author: shen@mmk.su.se (Z. J. Shen)

Abstract. With selective laser melting the potential to manufacture a wide variety of geometries from different materials has presented itself. Interest in this technology keeps growing every year, and with that growth a deeper understanding of the process and resulting materials is urgently needed. In this paper we present a short overview of the structural elements that appear during selective laser melting, and explain how to tailor them to achieve specific structures and material properties. Melt-pools, texture and grains, subgrain cells, and inclusions are the elements discussed herein, and tailoring of these elements can have effects on density, and corrosion resistance, as well as mechanical properties in general.

1. Introduction

Additive manufacturing (AM) has in the last decades become a broad field, covering many different techniques the manufacture of parts [1]. The number of materials that can be used in AM is also rising and today materials such as metals, polymers, ceramics, and wax can all be utilized [2,3]. AM is based on a layer-by-layer processing principle where each layer of solid material is added on top of the previous one. In this way, a three-dimensional part is built up from the bottom to the top, one layer at a time. A computer-aided design (CAD) file is loaded into the controlling computer and is then followed by the machine to get the desired size and geometry of the parts. This design process gives excellent control over the resulting shape in a way that cannot be easily achieved by conventional manufacturing methods. This makes the process ideal for rapid prototyping [4,5]. In the early days of additive manufacturing, fast prototyping was indeed the central focus of the technology, but nowadays many different industries and companies are starting to realize the possibilities of the technique for production of real parts [6]. Such industrial sectors as aerospace [7,8], automotive [9], biomedical [10–12] and energy [13,14] are involved in the research on innovative additive manufacturing methods and applications.

Selective laser melting (SLM) is one of the possible methods in this category. A bed with powder is exposed to a high-energy laser beam that melts the powder granules and forms a solid part. This manufacturing method gives rise to several different structural elements that need to be fully understood. Melt pools, grains, sub-grains, and inclusions are some of the essential characteristics of SLM-manufactured materials. In this article, these elements are given a short explanation together

with tailoring possibilities and we discuss how resulting changes in structure can impact different aspects of the performance of the SLM-manufactured material.

2. Melt pools

Melt pools are one of the hierarchically highest levels of the structure observed in SLM-manufactured material. This structural feature is something that is only found when using the powder bed fusion type of additive manufacturing to produce parts. They form around the spot where the laser, or other beam used to melt the material, hits the material and give a distinct appearance when they solidify. The size and form of these melt pools can readily be manipulated by the different parameters that control the laser beam. These parameters include (*i*) the power of the laser, (*ii*) the distance between each scanning track (also called hatch distance), (*iii*) the layer thickness, and (*iv*) the scanning speed of the laser. If the machine is using a discontinuous laser, the scanning speed is replaced by exposure time and the distance between exposure points.

2.1.Density

Melt pool dynamics and size also have a tremendous impact on the density of the manufactured material [15]. When heating up the material surface using a high-energy laser the center point gets much hotter than the surrounding material, which induces complex motions in the melt. Other driving forces for melt motion are laser-induced vapor plumes and plasma. These effect the melt by leading to the formation of an uneven surface after it cools down and solidifies. Parameter optimization to form bigger melt pools will decrease the effect of flow in the melt pool on surface roughness and thus increase the density. Good overlap of the melt pools is also crucial to get a smooth and fully dense material. If the melt tracks do not have enough overlap, un-melted powder granules may be present in the finished part (figure 1).

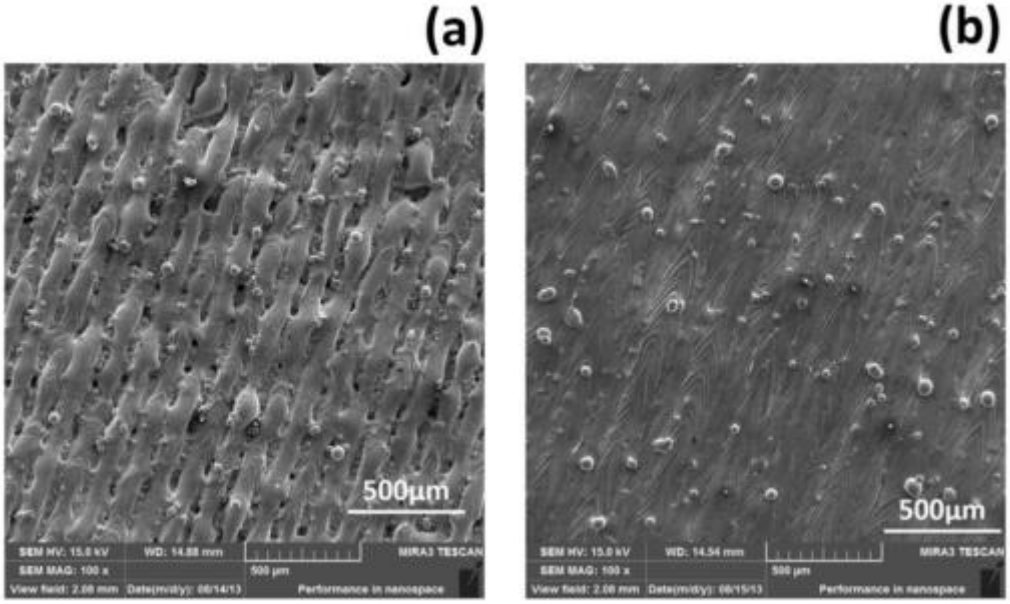

Figure 1. Scanning electron microscopy (SEM) images that show the surface morphologies of the Co-Cr-Mo alloy samples manufactured with different laser powers: (a)130W, showing a lack of overlap between melt tracks and (b) 200W, showing a smooth surface. Other parameters applied: hatch distance 125µm and laser speed 700 mm/s[15].

2.2.Corrosion resistance

Corrosion resistance is one material property that is critical in for example biomedical applications. Tailoring this property is possible for CoCrMo alloys manufactured with SLM. Using three different scanning parameters, where all of them were optimized for full density, and comparing the results to

conventionally cast material, it is observed that all the samples manufactured with SLM have higher resistance to corrosion and lower metal release than the cast sample [11]. It can also be seen that changing the parameters, and in effect changing the melt pools forms and sizes, can to some extent alter the amount of metal released and the corrosion resistance. The likely reason for this behavior is that the melt pool boundaries are weaker to corrosion. A more evident finding is the difference in corrosion resistance when using combined potentiodynamic polarization. The difference between the different SLM-manufactured samples are in this case more apparent, and a clear trend can be observed where a higher amount of melt pool boundaries present on the top plane leads to less passivization of the material (figure 2). There are also more spikes in the the curves for samples containing more melt pool boundaries, which also implies lower corrosion resistance.

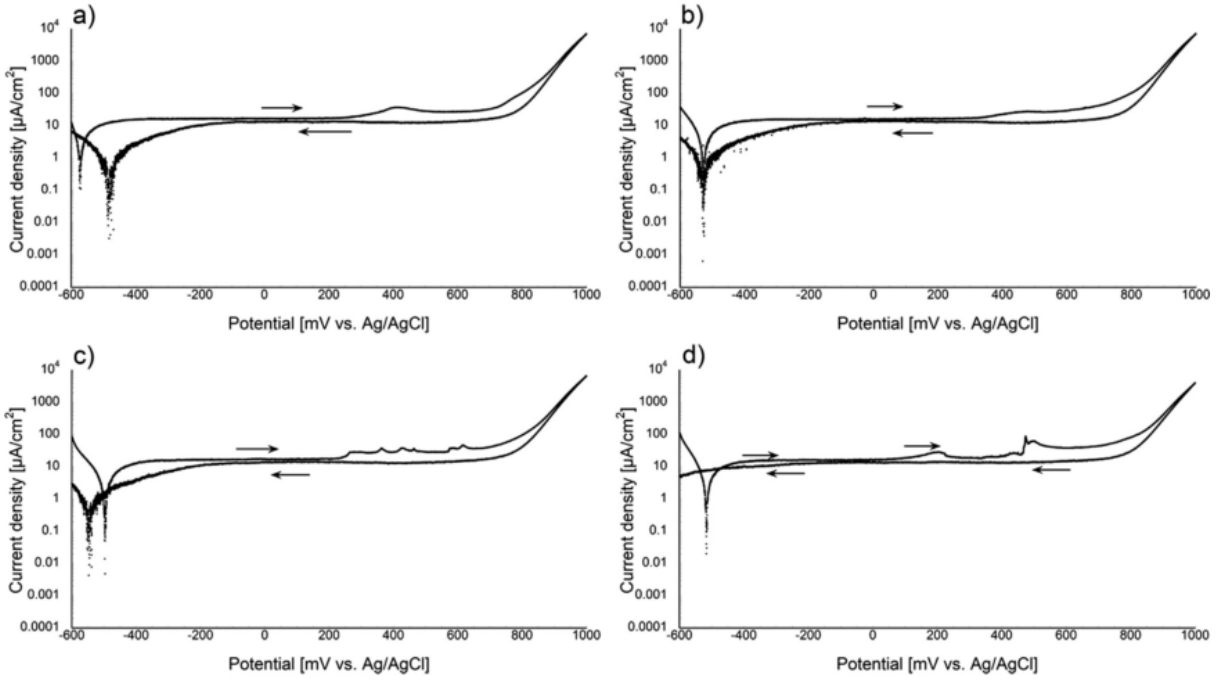

Figure 2. Potentiodynamic polarization (vs. Ag/AgCl) of SLM parts with an increase in melt-pool boundaries on the upper surface (a-c) and a conventionally cast part (d).[11]

3. Texture and Grains

During SLM process, the grains in the previous layer act as the nucleation sites for the further solidification of the melt through heterogeneous nucleation without altering crystallographic orientation, i.e., an epitaxial growth situation. Due to the directional solidification, the grains tend to grow along the temperature gradient direction with a preferred orientation. The morphological texture and crystallographic texture can both be tuned by adjusting processing parameters in CoCr alloy, specifically the scanning strategy, the hatch spacing, and the scanning speed.

The scanning strategy is important because the temperature gradient direction is determined by the laser scanning direction. If the laser is not rotated in adjacent layers, the grains tend to grow not only in the natural growth direction <100> but also the <110> direction on the outermost plane, and they tend to grow much stronger in the <100> direction along the scanning direction in the bulk material. The columnar grains are larger and distinguishable in this case. If the laser is rotated 67° in adjacent layers, the crystallographic texture is much weaker, and the grains are generally much smaller (figure 3). The grain growth direction becomes more random by changing the laser direction after each layer, so the columnar directional microstructure is fragmented under the induced complex thermal field.

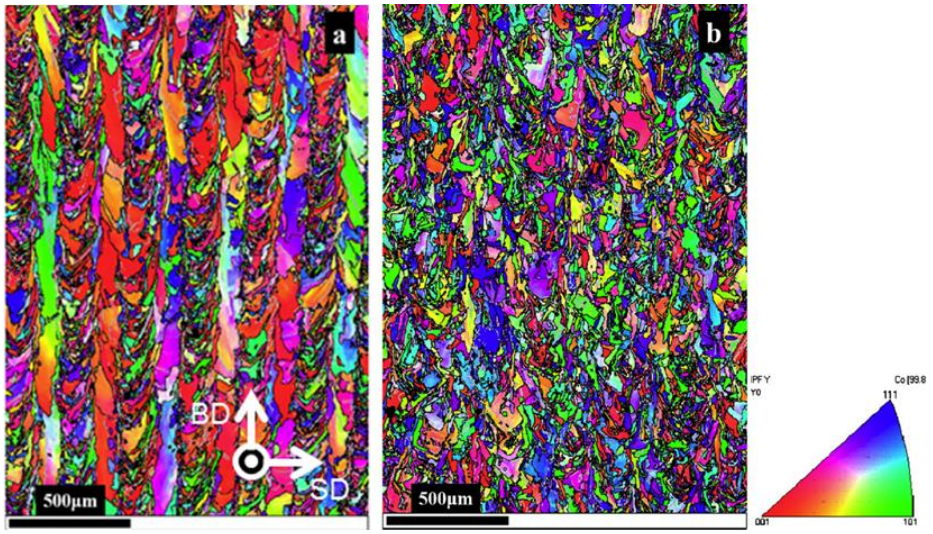

Figure 3. Electron backscatter diffraction (EBSD) orientation maps on the side plane of a CoCr sample consolidated by SLM with laser rotated 0° (a) and 67° between layer (b) [16]. Rotating the direction of laser scanning between layers results in a weaker texture and smaller grains.

The hatch spacing can also be used to tune the grain morphology and texture. Normally there are small equiaxed grains in the center line of melt tracks due to constitutional supercooling. These equiaxed grains can be removed by decreasing the hatch spacing as seen in figure 4. With the small hatch spacing shown in figure 5a, the adjacent melt tracks are firmly bonded, and the epitaxial grain growth diminishes the fusion line. The larger heat input generates lower G×R value (where G is the temperature gradient, and R is the grain growth rate) and thus results in larger grains and a stronger texture, which in turn results from epitaxial grain growth. The new melt track cannot re-melt the previous one, and thus a random distribution structure is retained with larger hatch spacing, as seen in figure 5b.

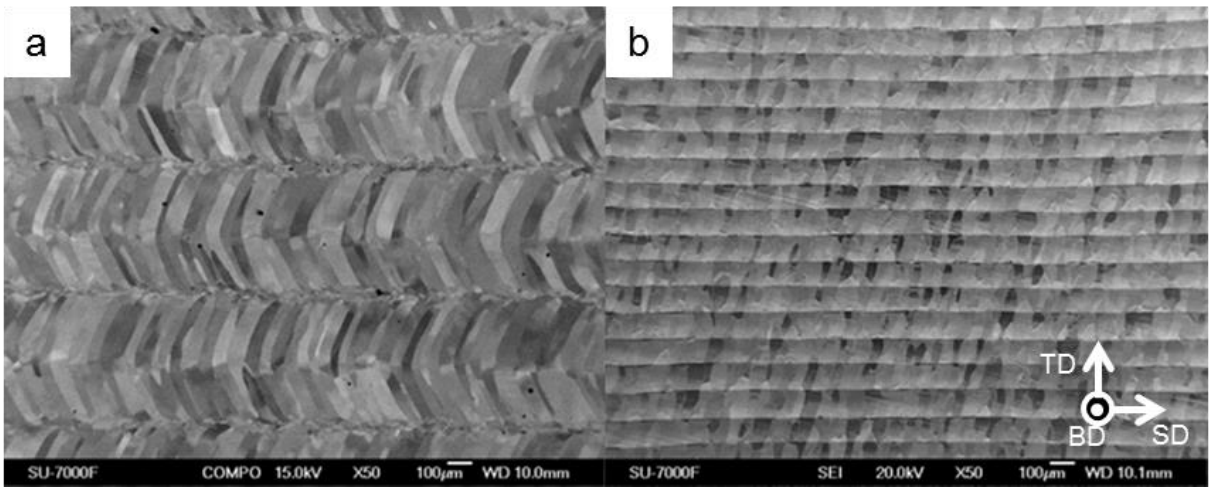

Figure 4. SEM image of melt tracks of Tungsten consolidated with large hatch spacing (a) giving rise to equiaxed grains, and small hatch spacing (b) where no equiaxed grains can be seen.

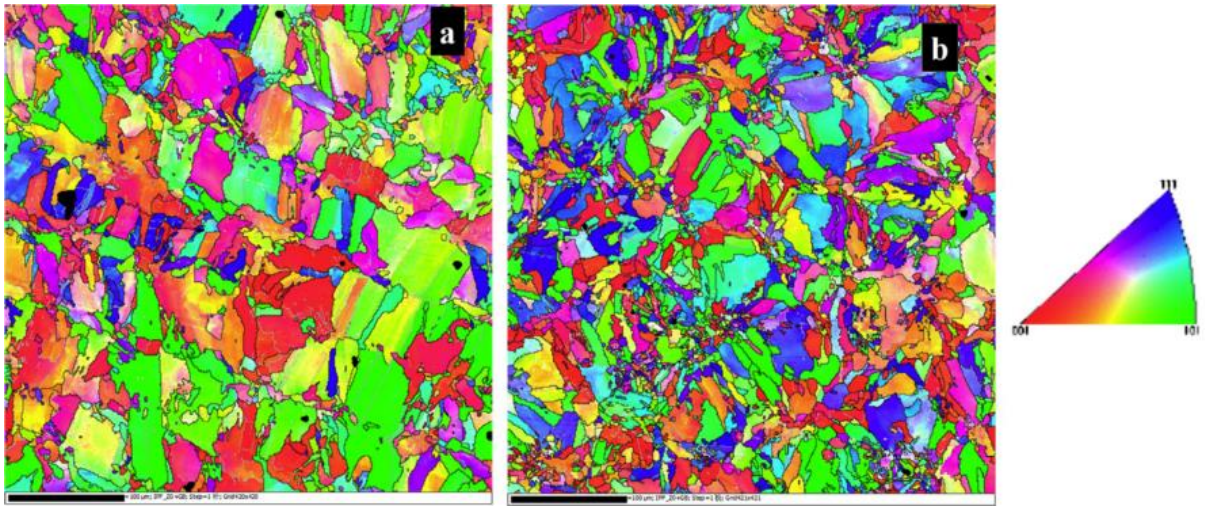

Figure 5. EBSD orientation maps on the top plane of SLM CoCr with hatch spacing 60 µm (a) and 175 µm (b) [16]. In (a) an overlap of the melt pools occurs and thus remelting of the smaller grains, allowing for epitaxial grain growth.

Higher scanning speeds result in a faster solidification rate and a shallow and elongated melt pool shape, which gives rise to a <001> growth preference from the previous layer into the present layer. This can result in a stronger texture [17].

4. Subgrain cellular structure

Subgrain features are found inside the grains of 316LSS manufactured by SLM. Scanning electron microscope (SEM) images of the etched surface of SLM-manufactured 316LSS shows a cellular structure with the cell boundaries less etched and the inside of the cells more etched (figure 6). The cells are around 500 nm in diameter, although the diameter varies in different regions. In most of the cases, spherical cells or elliptical cells are found, but tube like features may also form. This implies that the cells are columnar in shape. The lengths of the columnar cells can be up to hundred micrometers, which is much longer than the size in the other two dimensions.

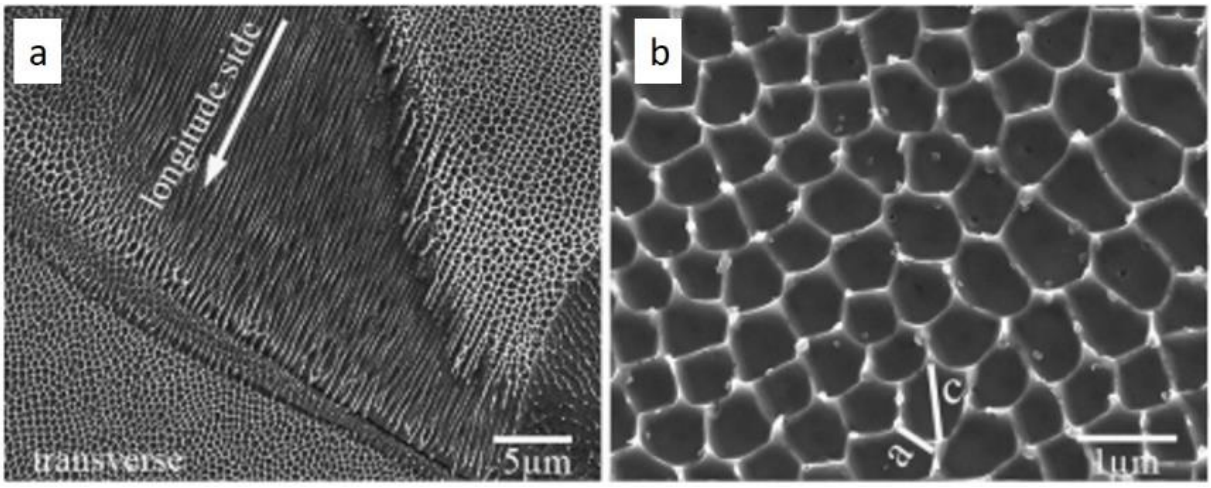

Figure 6. (a) low magnification SEM image of the etched surface of SLM- manufactured 316LSS showing the cellular structure from both the longitudal and radial cross-sections; (b) High magnification SEM image showing the average diameter of the cells of around 500 nm [18].

The cell boundaries are more corrosion resistant than the insides of the cells, resulting in the difference of the contrast in the SEM images. The difference in corrosion resistance is probably due to differences in the compositions. As shown in figure 7, the boundaries of the cells show lighter contrast than the inner part in the dark field scanning transmission electron microscopy (DF-STEM) images, implying the segregation of heavy elements at the boundaries. This is also confirmed by energy-dispersive X-ray spectroscopy (EDS) maps of the Cr distribution.

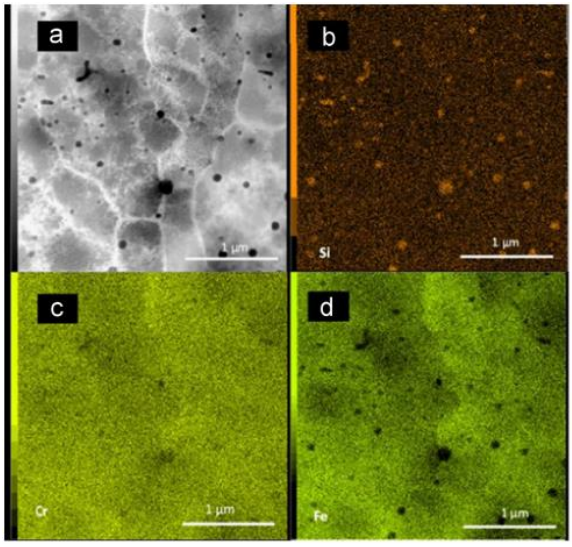

Figure 7. (a) DF-STEM image of the subgrain cellular structure; (b-d) EDS maps of the Si, Cr and Fe elements[19].

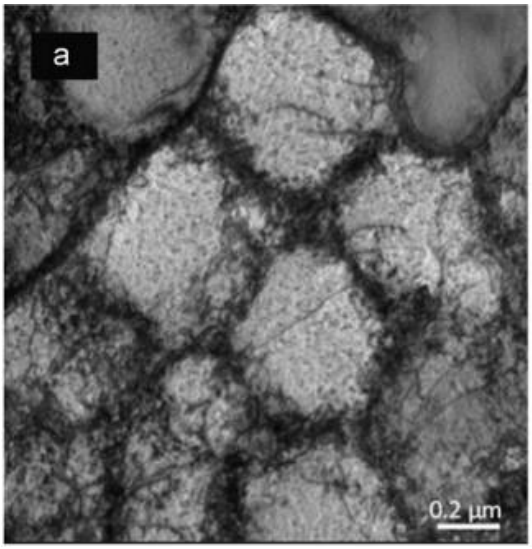

Figure 8. BF-TEM image of SLM-manufactured 316LSS showing the distribution of dislocations at the cell boundaries [19].

Besides the segregation of heavy elements, dislocations are often found to concentrate at the cell boundaries. In the bright field (BF) TEM image in figure 8, the dislocations are shown as dark lines. It is found that there are a few dislocations in the inner part of the cells while a high density of dislocations can be found at the boundaries.

Dislocations are line defects known to have a significant effect on the mechanical properties of metallic materials. The high density of dislocations stored in the structure can effectively increase the critical shear stress for dislocation motion, and hence introducing dislocations is often used for improving the strength of metals in conventional metal processing techniques e.g. rolling and drawing. In the SLM-manufactured 316LSS, the subgrain structure results in a high density of dislocations in the grains. As expected, the yield strength of the SLM-manufactured sample is notably higher than the annealed counterpart.

The formation of the subgrain structure is closely related to the process condition during SLM. Therefore, by changing the process parameters, it should be possible to alter the size and configuration of the subgrain cellular structure and thus the strength of the metal. This means that even in the same sample different regions could have different strengths, by tailoring the local subgrain cellular structure.

5. Oxide dispersion strengthening

The size of *in-situ* formed nano-inclusions can be adjusted by changing the oxygen partial pressure in the processing chamber. Almost no nano-inclusions can be observed in specimens consolidated in an extremely low oxygen chamber environment, as seen in figure 9a,b. By increasing the oxygen level to 300-500 ppm, large particles with size 2 µm are formed. Nevertheless, further increasing oxygen level to 1000-1200 ppm leads to smaller nano-inclusions with size around 50 nm. The higher oxygen level

in the laser chamber results in a higher dissolved oxygen in the melt, and thus a larger number of oxide particles that can be generated. At a high level (1000-1200 ppm), the maximum radius of nano-inclusions is controlled by the shorter diffusion radius R_d due to the higher density of the initial reactive cores as seen in figure 10. In the medium level range (300-500 ppm), the nano-inclusions can grow larger due to the smaller number of oxide particles and the longer value of R_d.

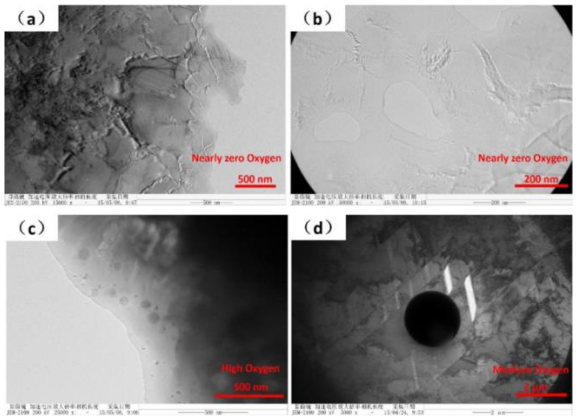

Figure 9. Distribution of oxide particles in stainless steel 316L, chamber oxygen level of less than 50 ppm (a,b), 1000-1200 ppm (c), 300-500 ppm (d) [20]

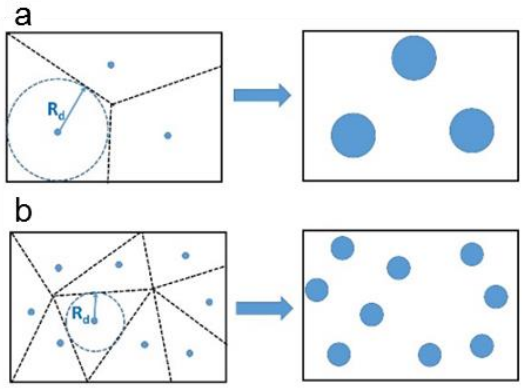

Figure 10. Oxide nano-inclusion growth in medium oxygen level 300-500 ppm (a) and high oxygen level 1000-1200 ppm (b) [20]

6. Conclusions and perspectives

Several different conclusions can be drawn about the possibility to tailor the microstructure to achieve desired properties for materials manufactured by selective laser melting.

1. By manipulating the size and shape of the melt pools it is possible to reach full density in materials, but also to lower the density if that is desirable. The corrosion resistance of the SLM-manufactured materials can also correlate with the melt pools size in such a way that a smaller area of melt-pool boundaries only at the surface exposed to an oxidizing environment will lead to better corrosion resistance and less metal release.
2. Grains tend to grow in the direction of the temperature gradient of the melt pool. By changing the scanning strategy the growth pattern and final size of the grains can be manipulated.
3. Cellular structures may also form in some cases consisting of dislocation networks that can help improve the mechanical properties of the material.
4. By monitoring and controlling the oxygen level in the building chamber, the size of *in-situ* formed oxide inclusions can be tailored.

The broad challenges for future work are twofold. The first is to find other characteristics of both microstructure and properties of the material that can be tailored by control of the SLM manufacturing conditions. The second, is to improve current methods of tailoring the structure and properties to achieve better control and more reliable results. In these ways, materials with better properties and/or improved performance than their conventional counterparts can be developed by selective laser melting.

References

[1] Wong K V and Hernandez A 2012 A Review of Additive Manufacturing *ISRN Mech. Eng.* **2012** 1

[2] Calignano F, Manfredi D, Ambrosio E P, Biamino S, Lombardi M, Atzeni E, Salmi A, Minetola P, Iuliano L and Fino P 2017 Overview on Additive Manufacturing Technologies *Proc. IEEE* **105** 593

[3] Frazier W E 2014 Metal additive manufacturing: A review *J. Mater. Eng. Perform.* **23** 1917

[4] Karunakaran K P, Bernard A, Suryakumar S, Dembinski L and Taillandier G 2012 Rapid manufacturing of metallic objects *Rapid Prototyp. J.* **18** 264
[5] Campbell I, Bourell D and Gibson I 2012 Additive Manufacturing: Rapid Prototyping comes of age *Rapid Prototyp. J.* **18** 255
[6] Guo N and Leu M C 2013 Additive manufacturing: Technology, applications and research needs *Front. Mech. Eng.* **8** 215
[7] Liu R, Wang Z, Sparks T, Liou F and Newkirk J 2017 *13 – Aerospace applications of laser additive manufacturing* (Elsevier Ltd)
[8] Shapiro A A, Borgonia J P, Chen Q N, Dillon R P, McEnerney B, Polit-Casillas R and Soloway L 2016 Additive Manufacturing for Aerospace Flight Applications *J. Spacecr. Rockets* **53** 952
[9] Leal R, Barreiros F M, Alves L, Romeiro F, Vasco J C, Santos M and Marto C 2017 Additive manufacturing tooling for the automotive industry *Int. J. Adv. Manuf. Technol.* 1
[10] Yadroitsev I, Krakhmalev P and Yadroitsava I 2014 Selective laser melting of Ti6Al4V alloy for biomedical applications: Temperature monitoring and microstructural evolution *J. Alloys Compd.* **583** 404
[11] Hedberg Y S, Qian B, Shen Z, Virtanen S and Odnevall Wallinder I 2014 In vitro biocompatibility of CoCrMo dental alloys fabricated by selective laser melting *Dent. Mater.* **30** 525
[12] Qian B, Saeidi K, Kvetková L, Lofaj F, Xiao C and Shen Z 2015 Defects-tolerant Co-Cr-Mo dental alloys prepared by selective laser melting *Dent. Mater.* **31** 1435
[13] Zhong Y, Rännar L-E, Wikman S, Koptyug A, Liu L, Cui D and Shen Z 2017 Additive manufacturing of ITER first wall panel parts by two approaches: Selective laser melting and electron beam melting *Fusion Eng. Des.* **116** 24
[14] Zhong Y, Rännar L-E, Liu L, Koptyug A, Wikman S, Olsen J, Cui D and Shen Z 2017 Additive manufacturing of 316L stainless steel by electron beam melting for nuclear fusion applications *J. Nucl. Mater.* **486** 234
[15] Zhou X, Wang D, Liu X, Zhang D D, Qu S, Ma J, London G, Shen Z and Liu W 2015 3D-imaging of selective laser melting defects in a Co-Cr-Mo alloy by synchrotron radiation micro-CT *Acta Mater.* **98** 1
[16] Zhou X, Li K, Zhang D, Liu X, Ma J, Liu W and Shen Z 2015 Textures formed in a CoCrMo alloy by selective laser melting *J. Alloys Compd.* **631** 153
[17] Dehoff R R, Kirka M M, Sames W J, Bilheux H, Tremsin A S, Lowe L E and Babu S S 2015 Site specific control of crystallographic grain orientation through electron beam additive manufacturing *Mater. Sci. Technol.* **31** 931
[18] Zhong Y, Liu L, Wikman S, Cui D and Shen Z 2016 Intragranular cellular segregation network structure strengthening 316L stainless steel prepared by selective laser melting *J. Nucl. Mater.* **470** 170
[19] Saeidi K, Gao X, Zhong Y and Shen Z J J 2015 Hardened austenite steel with columnar sub-grain structure formed by laser melting *Mater. Sci. Eng. A* **625** 221
[20] Zhou X, An Z, Shen Z, Liu W and Yao C 2017 Particles control in selective laser melting in-situ oxide dispersion strengthened method *IOP Conf. Ser. Mater. Sci. Eng.* **167**